Materials Today Bio 32 (2025) 101673

Contents lists available at ScienceDirect

Materials Today Bio

journal homepage: www.journals.elsevier.com/materials-today-bio

Improved pleiotropic antibacterial activity of Ag(I)-Thiolate coordination polymers via iodide encapsulation in multinuclear silver nano cages

Chunhong Tan [a,1], Menghan Lu [b,1], Tao Zhou [a], Zhen Fang [c], Juan Zhou [d], Xiao-Feng Wang [a,*], Guoqing Wang [b,**], Ying-Wu Lin [a,***], João Rocha [e,****]

[a] School of Chemistry and Chemical Engineering, University of South China, Hengyang, 421001, China
[b] Institute of Evolution and Marine Biodiversity, and College of Food Science and Engineering, Ocean University of China, Qingdao, China
[c] College of Chemistry and Materials Science, Anhui Normal University, Wuhu, 241000, China
[d] College of Mechanical Engineering, University of South China, Hengyang, 421001, China
[e] CICECO-Aveiro Institute of Materials, Department of Chemistry, University of Aveiro, 3810-193, Aveiro, Portugal

ARTICLE INFO

Keywords:
Coordination polymer
Silver nano-cage
Iodide
Antimicrobial
Synergistic mechanism

ABSTRACT

Silver-based nanomaterials have attracted considerable attention due to their antimicrobial properties. In this study, two nano-Ag^{I}-cage-based coordination polymers, $[Ag_6(\mu\text{-}StBu)_6]_n$ (University of South China Coordination Polymer USC-CP-2) and $[Ag_{14}(\mu\text{-}StBu)_{12}I_2]_n$ (USC-CP-3), were synthesized via the reaction of $AgNO_3$ and 2-methyl-2-propanethiol (HS*t*Bu) with sodium ethylate as a non-toxic base in a water/ethanol mixed solvent, with and without iodide as a coligand. Structural analysis by single-crystal X-ray diffraction revealed that both polymers are one-dimensional Ag(I)-thiolate coordination polymers with distinct secondary building units: USC-CP-2 features Ag_6 nano-cages stabilized by μ_2-S*t*Bu ligands, while USC-CP-3 comprises nanochains formed by iodide-encapsulated Ag_{16}-cages linked through edge-sharing. Antimicrobial studies against *Escherichia coli* demonstrated that USC-CP-3, featuring iodide-encapsulated Ag_{16}-cages, exhibited superior antibacterial activity compared to the iodide-free Ag_6-cages in USC-CP-2. Mechanistic studies, supported by ICP-MS, EPR, TEM, and SEM analyses, suggested that the synergistic bactericidal effects arise from the release of Ag(I) ions, hydroxyl radical generation, and the presence of iodide. This study highlights a rational design strategy for advanced antibacterial materials with potential applications in combating bacterial contamination.

1. Introduction

Human and animal health face significant hazards from harmful microorganisms, particularly due to persistent infections caused by multidrug-resistant bacteria, biofilm formation, and the spread of foodborne pathogens [1–4]. According to the World Health Organization, antimicrobial (AMR) resistance is one the most pressing global public health and development threats, directly responsible for 1.27 million deaths worldwide in 2019, surpassing even cancer as a leading cause of mortality [5–7]. This highlights the urgent need to develop effective antibacterial agents. Despite the introduction of numerous antibacterial materials, including organic, inorganic and hybrid agents [8–23], critical challenges remain: (i) toxicity and irritancy, (ii) generation of undesirable by-products, and (iii) increasing bacterial resistance to existing treatments [24–26]. These issues highlight the need for further research into nanomaterials with enhanced disinfection properties and reduced drawbacks.

Silver ions are well-known for their broad-spectrum bactericidal properties, combining high efficacy against bacteria fungi, and viruses with relatively low toxicity toward mammalian cells [16–20,27,28]. To date, thousands of silver-based antimicrobial agents have been patented [29,30], reflecting their versatility and effectiveness. Their antibacterial activity is primarily attributed to mechanisms such as physical contact, release of silver ions, oxidative stress, and photothermal effects [31,32].

* Corresponding author.
** Corresponding author.
*** Corresponding authors.
**** Corresponding author.
E-mail addresses: xfwang518@sina.cn (X.-F. Wang), gqwang@ouc.edu.cn (G. Wang), ywlin@usc.edu.cn (Y.-W. Lin), rocha@ua.pt (J. Rocha).
[1] These authors contributed equally.

https://doi.org/10.1016/j.mtbio.2025.101673
Received 10 January 2025; Received in revised form 13 March 2025; Accepted 15 March 2025
Available online 19 March 2025

Silver nanoparticles (Ag-NPs) are particularly promising due to their synergistic effects and adaptability, but they face limitations such as aggregation, and environmental release, which pose health risks such as argyria or argyrosis (chronic disorders affecting skin microvessels and eyes) [33–35]. To address these limitations, Ag(I) coordination complexes have emerged as superior alternatives. These complexes ensure efficient physical contact with bacteria, promote membrane rupture, and offer tunable structures for controlled release of silver ions and organic linkers [17–20]. Their high crystallinity allows precise determination of intrinsic structures, enabling rational design and optimization for specific applications [16,36].

According to the Lewis rule of hard and soft acids and bases, Ag(I), classified as a soft acid, exhibits a strong affinity for soft bases, particularly sulfur compounds. Coordination complexes with S-donor ligands demonstrate greater stability compared to N- and O-donor ligand-based systems, making them ideal for long-lasting antibacterial agents [37–40]. The bactericidal mechanism of Ag(I) coordination complexes primarily involves the release of silver ions, which trigger multiple biophysical disruptions in bacteria. These disruptions include binding to enzymes or DNAs, blocking phosphate uptake and exchange, and altering proton transmembrane behavior, ultimately leading to bacterial inactivation [1–5].

As illustrated in Scheme 1, the Ag-S bonding enables the formation of diverse structural ensembles with significant flexibility [39,40], ranging from discrete Ag(I)-thiolate clusters [41–43] to high-dimensional Ag (I)-thiolate coordination polymers, including 1-D chains, 2-D lamellar structures, and 3-D frameworks [44]. Given the urgent need for effective antibacterial agents in combating multidrug-resistant bacteria, biofilm formation, and foodborne pathogens, silver-thiolate materials offer a promising alternative to conventional treatments. Their antibacterial efficacy primarily stems from the controlled release of silver ions, a critical factor in balancing bactericidal efficiency and longevity, while minimizing the drawbacks associated with silver nanoparticles, such as aggregation and potential toxicity [16–20,27,28].

Among Ag(I)-thiolate coordination polymers, the chain-type structures emerge as particularly attractive candidates for practical applications. They offer a higher effective Ag(I) content per unit compared to 2-D layers or 3-D frameworks, ensuring potent antimicrobial activity, while also providing better dispersibility than discrete Ag(I)-thiolate clusters [45]. Their well-defined crystalline nature enables rational structural tuning, allowing optimization for sustained silver ion release and enhanced antibacterial performance. These properties align with the growing demand for nanomaterials that not only exhibit superior disinfection capabilities but also mitigate resistance development, making Ag(I)-thiolate coordination polymers a compelling direction for next-generation antimicrobial solutions.

Additionally, iodine, an efficient and inexpensive biocide, enhances antibacterial efficacy by causing irreversible damage to microbial cells [46–48]. However, few studies have explored iodide-encapsulated Ag-coordination polymers, leaving a gap in understanding the synergistic effects of sulfur and iodide ligands.

To address this, two double-stranded chain-type Ag(I)-thiolate coordination polymers (with and without iodide incorporation) were synthesized using a hydro-solvothermal method (Scheme 2). Structural analysis revealed the formation of multi-Ag(I) nanocages: $[Ag_6(\mu\text{-}StBu)_6]_n$ (University of South China Coordination Polymer USC-CP-2) and $[Ag_{14}(\mu\text{-}StBu)_{12}I_2]_n$ (USC-CP-3).

Both exhibited significant antibacterial activity against *Escherichia coli*, a clinically relevant pathogen selected for its prevalence and role in infections. USC-CP-3 outperformed USC-CP-2 due to a synergistic mechanism involving Ag(I) release, radical generation, and iodide ions. These findings highlight the potential of 1-D Ag(I)-thiolate coordination polymers as promising antibacterial nanocomposites, with their composition and nanocage microstructure offering opportunities for optimization. This study validates a rational design strategy for developing efficient antibacterial agents.

2. Experimental

2.1. Materials and methods

All reagents and solvents were obtained from commercial suppliers and used without further purification. Elemental analyses (C, H, and N) were performed on a Vario MICRO CHNOS Elemental Analyzer. Powder X-ray diffraction data were collected on a DMAX-2500 diffractometer using CuKα. Thermogravimetric analyses were carried out on a NETZSCH TG 209F3 instrument in an N_2 atmosphere. Infrared absorption spectra were measured on a Fourier-transform infrared spectrometer (Bruker VERTEX 70) in the range of 400–4000 cm^{-1}. Electron paramagnetic resonance spectra were recorded on a Bruker A300

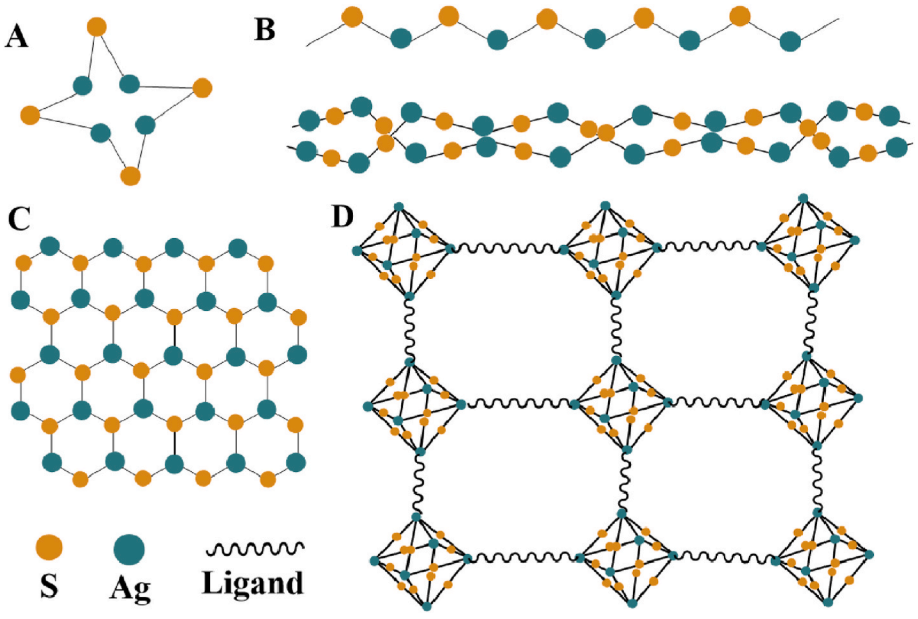

Scheme 1. Proposed configurations and arrangements of S and Ag atoms in Ag(I)-thiolate coordination complexes: (A) discrete clusters, (B) single chain and double-stranded chains, (C) 2-D networks, (D) 3-D coordination polymer.

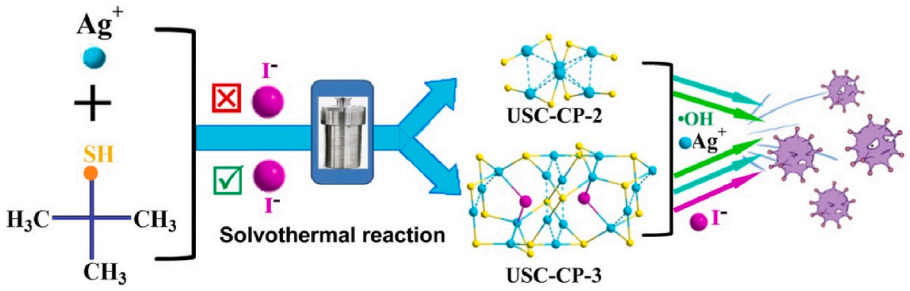

Scheme 2. Schematic representation of the synthesis and antibacterial properties of CP-2 and CP-3.

spectrometer (X-band) equipped with a Bruker ER4141VTM liquid nitrogen system. Transmission electron microscopy (TEM) images were taken using a JEOL JEM-2100 Plus field emission microscope. Scanning electron microscope (SEM) images were collected on a Hitachi Regulus8100 field emission scanning electron microscope. Electron paramagnetic resonance (EPR) spectra were recorded under white LED light irradiation for 5 min using DMPO as a radical scavenger (instrument model: EMXPLUS10/12). The Ag^+ content was quantified using inductively coupled plasma mass spectrometry (ICP-MS) with a NexION™ 350X ICP-MS.

2.2. Synthetic procedures

$[Ag_6(\mu\text{-}StBu)_6]_n$ (USC-CP-2) Sodium ethylate (0.028 g, 0.4 mmol) and 2-methyl-2-propanethiol (0.043 mL, 0.4 mmol) were dissolved in 6 mL of ethanol and stirred for 30 min. Subsequently, $AgNO_3$ (0.034 g, 0.2 mmol), dissolved in a mixture of 1 mL water and 2 mL ethanol, was added slowly to the solution. Upon addition, the solution turned milky white, and flocs began to form. The resulting turbid mixture was transferred to a 20 mL Teflon-lined autoclave and heated at 130 °C for 33 h. After cooling, strip-shaped colourless crystals of USC-CP-2 were isolated and repeatedly washed with water. Yield: 51 % (based on Ag). Elemental analysis - calculated for $Ag_6S_6C_{24}H_{54}$: C 24.38, H 4.60; found: C 24.32, H 4.72 %.

$[Ag_{14}(\mu\text{-}StBu)_{12}I_2]_n$ (USC-CP-3) Sodium ethylate (0.028 g, 0.4 mmol) and 2-methyl-2-propanethiol (0.043 mL, 0.4 mmol) were dissolved in 6 mL of ethanol and stirred for 30 min. $AgNO_3$ (0.034 g, 0.2 mmol), dissolved in 1 mL of water and 2 mL of ethanol, was then added in slowly to the solution. The mixture turned milky white and and flocs began to form. Subsequently, a mixture of potassium iodide (0.033 g, 0.2 mmol) in 2 mL of acetone and 1 mL of ethanol was added. The turbid mixture was transferred to a 20 mL Teflon-lined autoclave and heated at 130 °C for 33 h. Upon cooling, light yellow crystals of USC-CP-3 were isolated and repeatedly washed with water. Yield: 19 % (based on Ag). Elemental analysis - calculated for $Ag_7S_6C_{24}H_{54}I$: C 20.34, H 3.84; found: C 20.22, H 3.93 %.

2.3. X-ray crystallography

Single crystal data were collected on a Rigaku SCXmini CCD diffractometer equipped with graphite-monochromated Mo-Kα radiation source ($\lambda = 0.71073$ Å) in ω scan mode. The structures were solved by direct methods using the SHELXTL Version 5 software package and refined with a full-matrix least-squares refinement on F^2. Metal atoms were located from electron-density maps and refined anisotropically. Non-hydrogen atoms were located using difference Fourier maps based on initial atomic positions and were also refined anisotropically. Hydrogen atoms were added according to theoretical models. Crystal data and structure refinement details are provided in Table S1, while selected bonds lengths and angles are summarized in Tables S2 and S3, respectively.

2.4. Bacterial strains and culture conditions

To evaluate the antibacterial efficacy of the coordination polymers, *Escherichia coli* was selected as a representative bacterial strain due to its widespread use as a model organism in antimicrobial studies. Its well-characterized physiology and clinical relevance make it an ideal candidate for assessing the antibacterial performance of newly developed materials. *Escherichia coli* MG1655 was cultured in LB medium at 37 °C. The bacterial cell concentration was determined by measuring the absorbance of the suspension at 600 nm (OD_{600}) using a microplate reader (Varioskan Flash 3001, Thermo Fisher, USA).

2.5. Measurement of minimum inhibitory concentration (MIC)

The minimum inhibitory concentration of $[Ag_6(\mu\text{-}StBu)_6]_n$ (USC-CP-2) and $[Ag_{14}(\mu\text{-}StBu)_{12}I_2]_n$ (USC-CP-3) against *Escherichia coli* (*E. coli*, MG1655) was determined using the flatbed coating method. Briefly, varying amounts of USC-CP-2 and USC-CP-3 powders were added to LB nutrient agar medium, thoroughly mixed, and sterilized. The mixture was then poured into petri dishes and allowed to cool and solidify. *E. coli* cells were cultured in LB medium until reaching the logarithmic growth phase. A diluted bacterial suspension (10^4 CFU/mL, 30 μL) was evenly spread onto the prepared LB nutrient agar plates. The experiment involved two test groups: dark groups, in which samples were wrapped in tinfoil, and light groups, exposed to an LED lamp (0.7 mW/cm^2) positioned 30 cm above the petri dishes. To confirm that the antibacterial effects were specifically due to USC-CP-2 and USC-CP-3, bacterial suspensions without coordination polymers served as blank controls. These controls verified the normal growth and viability of *E. coli* under the experimental conditions. Both groups were incubated at 37 °C for 18 h, after which the remaining *E. coli* colonies were counted, and the results were expressed as colony-forming units per square centimeter (CFU/cm^2).

2.6. Electron microscopy characterizations of bacteria

The morphological changes of *Escherichia coli* before and after incubation with USC-CP-2 and USC-CP-3 were observed using SEM. *E. coli* was incubated with antibacterial agent (0.8 mg/mL) for 3 h, respectively. After incubation, the bacteria were collected by centrifugation (5000 rpm, 5 min) and fixed with 2.5 % glutaraldehyde (100 μL) for 12 h. The fixed bacterial cells were centrifuged at 5000 rpm for 5 min, and the resulting pellet was collected and washed three times with phosphate-buffered saline (PBS) to remove any residual fixative.

For TEM analysis, a fresh copper grid was hydrophilized using an ultraviolet ozone cleaner for 3–5 min. Then, 6–8 μL of the sample solution was deposited onto the grid and allowed to air dry. Morphological changes were observed using TEM at an operating voltage of 200 kV.

For SEM analysis, bacterial dehydration was performed after fixative removal. Briefly, the bacterial suspension was sequentially treated with 0.5 mL of ethanol solutions at concentrations of 30 %, 50 %, 70 %, 90 %, and 100 %, with each treatment lasting 15 min to ensure complete water

removal. After gold sputtering, the samples were imaged using SEM at an accelerating voltage of 5.0 kV.

2.7. Thermogravimetric analysis

Thermogravimetric analysis (TGA) was conducted to assess the thermal stability of USC-CP-2 and USC-CP-3. The coordination polymer crystalline powder was dried at 80 °C for 10 h to remove any residual solvent molecules. After drying, 3 mg of the powder was accurately weighed and placed in an Al_2O_3 pan. The sample was then heated from 50 °C to 650 °C at a rate of 10 °C/min, while nitrogen gas was continuously supplied at a flow rate of 25 mL/min throughout the TGA procedure.

2.8. Ag^+ release test

After overnight cultivation, the bacterial suspension was diluted 1:100 and further incubated for 2 h to reach the logarithmic growth phase. *E. coli* cells in this phase were treated with each antibacterial agent (0.8 mg/mL) and incubated at 37 °C for 2 h. The bacterial suspension was then centrifuged at 5000 rpm for 5 min and washed three times with phosphate-buffered saline (PBS) containing 0.1 % Triton X-100. After collection, the bacterial cells were lysed using an ultrasonic cell disruptor. The resulting lysates were digested with nitric acid, and silver absorption and uptake by the bacteria were quantitatively analyzed using ICP-MS.

2.9. Statistical analysis

All statistical data were obtained from at least three independent samples or replicates. A P-value of <0.05 was considered statistically significant.

3. Results and discussion

3.1. Structure characterization

Single-crystal X-ray diffraction analysis reveals that USC-CP-2 crystallizes in the triclinic system with the space group *P*1. As shown in Fig. 1 and Fig. S1, the asymmetric unit of the crystal structure comprises an Ag_6 cage containing six Ag atoms and six S*t*Bu bridging ligands. Each Ag atom is bonded to two sulfur atoms, adopting a linear geometry, with all sulfur atoms acting as μ_2-bridges. The Ag-S bond distances range from 2.369(2) to 2.400(1) Å, with an average length of 2.385 Å. The Ag···Ag separations range from 3.059(6) to 3.336(7) Å, which are slightly longer than the Ag···Ag separation in metallic silver (2.889 Å) but considerably shorter than the sum of the van der Waals radii (3.44 Å) [26], indicating the existence of weak metal-metal interactions. Each Ag_6-cage is connected to adjacent clusters through two μ_2-S*t*Bu bridging ligands, forming an infinite chain structure. These chains are further stacked together by weak intermolecular forces, resulting in a 3-D supramolecular aggregate.

USC-CP-3 crystallizes in the monoclinic system with the space group $P2_1/C$. As shown in Fig. 2 and Fig. S2, the asymmetric unit consists of seven Ag atoms, six S*t*Bu bridging ligands, and one I^- anion. The latter resides within the Ag_{16}-cage, adopting a triangular pyramid geometry by coordinating with three silver(I) atoms, with Ag···I distances ranging from 2.991(2) to 3.256(1) Å. Six silver atoms in the Ag_{16}-cage are bonded to three sulfur atoms and one iodide ion, forming a distorted tetrahedral AgS_3I geometry. The remaining ten silver atoms are bonded to two sulfur atoms, forming a V-shaped AgS_2 geometry. The sulfur atoms from the thiol ligands primarily act as μ-3 bridges, with one serving as a μ-2 bridge. The Ag-S bond distances range from 2.269(6) to 2.695(2) Å, with an average bond length of Ag-S of 2.444 Å. The Ag···Ag separations vary between 2.980(7) and 3.344(2) Å, indicating weak metal-metal interactions [26]. The Ag_{16}-cage is stabilized by sixteen 2-methyl-2-propanethiol ligands encasing its periphery. Adjacent Ag_{16}-cages are connected through edge-sharing, forming a continuous chain structure. These chains are stacked via weak intermolecular forces to create the 3-D supramolecular aggregate, USC-CP-3.

3.2. Structural comparisons and stability

The simulated and experimental powder X-ray diffraction patterns of USC-CP-2 and USC-CP-3, shown in Fig. 3, display consistent peak positions, confirming the phase purity of the products. This demonstrates the stability of the crystals, as they remain undamaged after being stored in a drawer for three months or immersed in water for half a month. In addition, thermogravimetric analysis (TGA) in N_2 reveals that all samples exhibit thermal stability up to 230 °C (Fig. 3). The weight loss observed beyond 250 °C is ascribed to the decomposition of the coordination polymer framework.

Although both coordination polymers form 1-D coordination polymeric structures through Ag-S coordination bonds and argentophilic

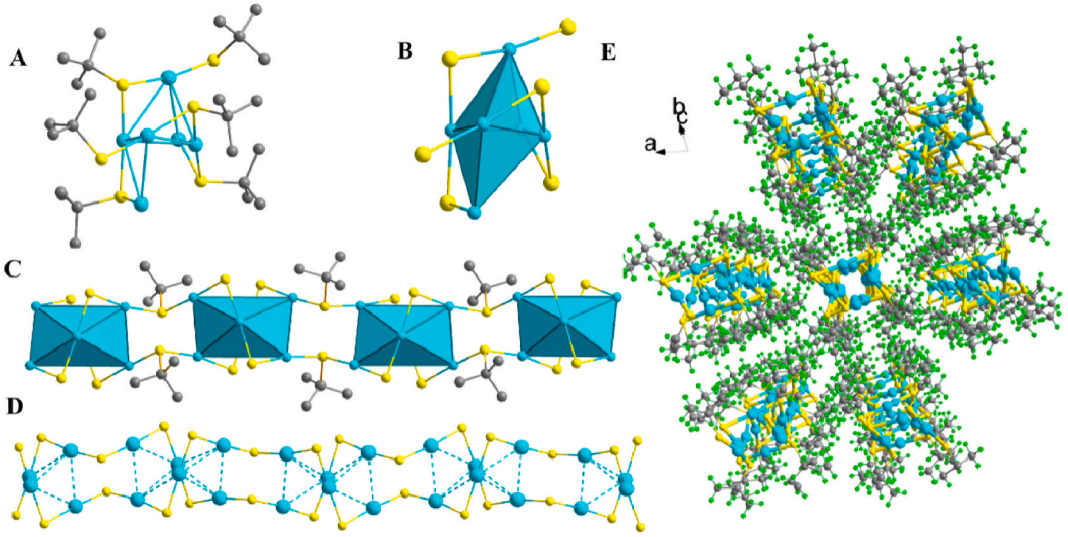

Fig. 1. (A) View of the asymmetric unit; (B) Structure of the Ag_6-cage; (C) 1-D chain structure formed by Ag_6-cages; (D) Representation of argentophilic interactions between individual chains; and (E) Packing arrangement of the chains in USC-CP-2 (Ag: turquoise, S: yellow, C: gray, H: bright green). (For interpretation of the references to colour in this figure legend, the reader is referred to the Web version of this article.)

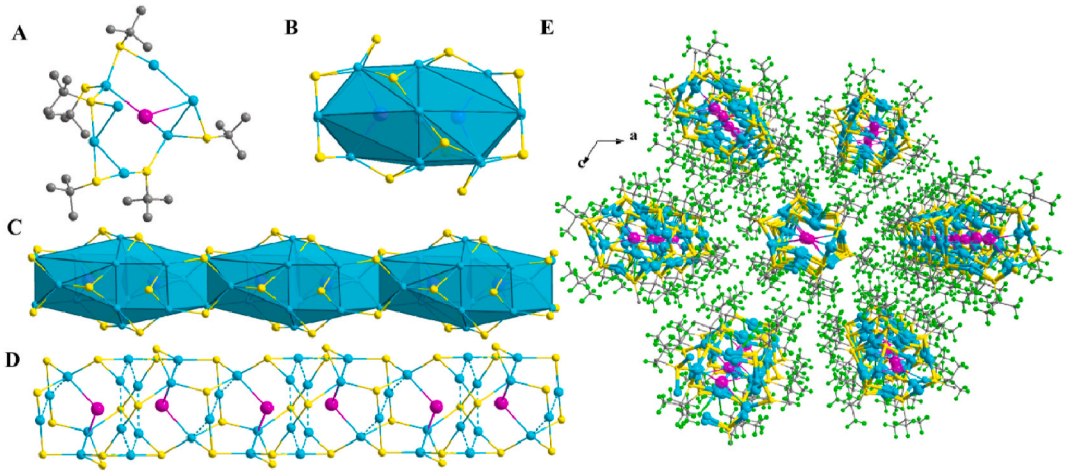

Fig. 2. (A) View of the asymmetric unit; (B) Structure of the Ag_{16}-cage stabilized by 2-methyl-2-propanethiol ligands; (C) 1-D chain structure formed by edge-shared Ag_{16}-cages; (D) Representation of the argentophilic interactions within the polymeric chain; and (E) Packing arrangement of the chains in USC-CP-3 (Ag: turquoise, S: yellow, I: purplish red, C: gray, H: bright green). (For interpretation of the references to colour in this figure legend, the reader is referred to the Web version of this article.)

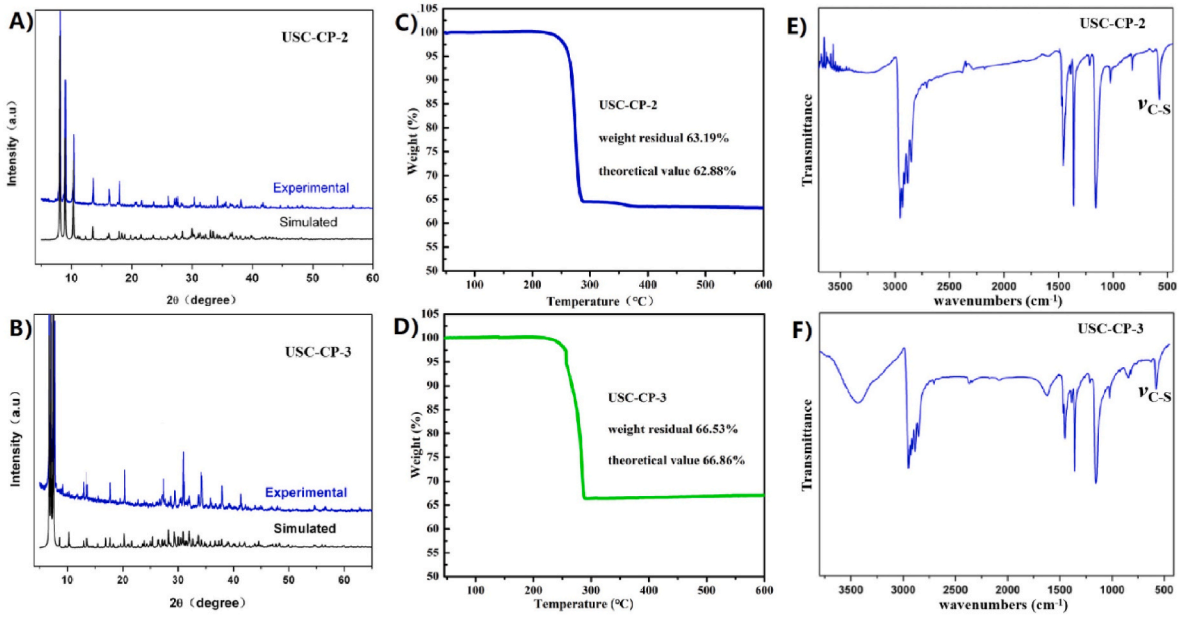

Fig. 3. (A), (B) powder X-ray diffraction patterns, (C), (D) TGA, and (E), (F) FT-IR spectra of USC-CP-2 and USC-CP-3.

interactions, the introduction of iodide results in a more complex structure with distinct building units and a greater variation in bond lengths for similar types of bonds. USC-CP-2 features sulfur-bridged, isolated Ag_6-cages in which the silver ions adopt an approximately linear coordination configuration. In contrast, USC-CP-3 consists of edge-shared Ag_{16}-cages, where the silver ions are in a tetrahedral coordination environment with a V-shaped geometry. These differences in building units, coordination numbers, and coordination configurations lead to variations in Ag-S bond lengths between the two coordination polymers. In USC-CP-2, the Ag-S bond distances within each isolated Ag_6-cage are consistently shorter than 2.4 Å (Table S2). However, in USC-CP-3, the Ag-S bond distances within each edge-shared Ag_{16}-cage are more diverse (Table S3). Only three Ag-S bonds are shorter than 2.4 Å, while the remaining thirty are longer than 2.5 Å, including two bonds measuring 2.669(2) and 2.695(2) Å. According to previously reported silver coordination polymers, the elongation of Ag-S bonds generally reduces their stability [32,49]. Consequently, the relatively lower stability of USC-CP-3 likely facilitates the release of more silver ions under identical conditions compared to USC-CP-2.

3.3. Antibacterial activity

The antibacterial efficacy of the coordination polymers against *Escherichia coli* was evaluated by their minimum inhibitory concentrations (MICs) using the agar diffusion method as well as the colony-forming units per square centimeter (CFU/cm^2) under both light and dark conditions. Due to their insolubility in water and most organic solvents, the antibacterial properties of the coordination polymers USC-CP-2 and USC-CP-3 were assessed in the form of finely ground crystal powders using a dilution plate coating test (35 mm × 10 mm) [16, 21–23,50]. As shown in Fig. 4A, the bacterial colony counts of *E. coli* on agar plates decreased continuously with increasing concentrations of CP-2 from 0 to 1.0 mg/mL under both dark and light conditions. Specifically, the remaining bacterial colony counts of *E. coli* decreased from

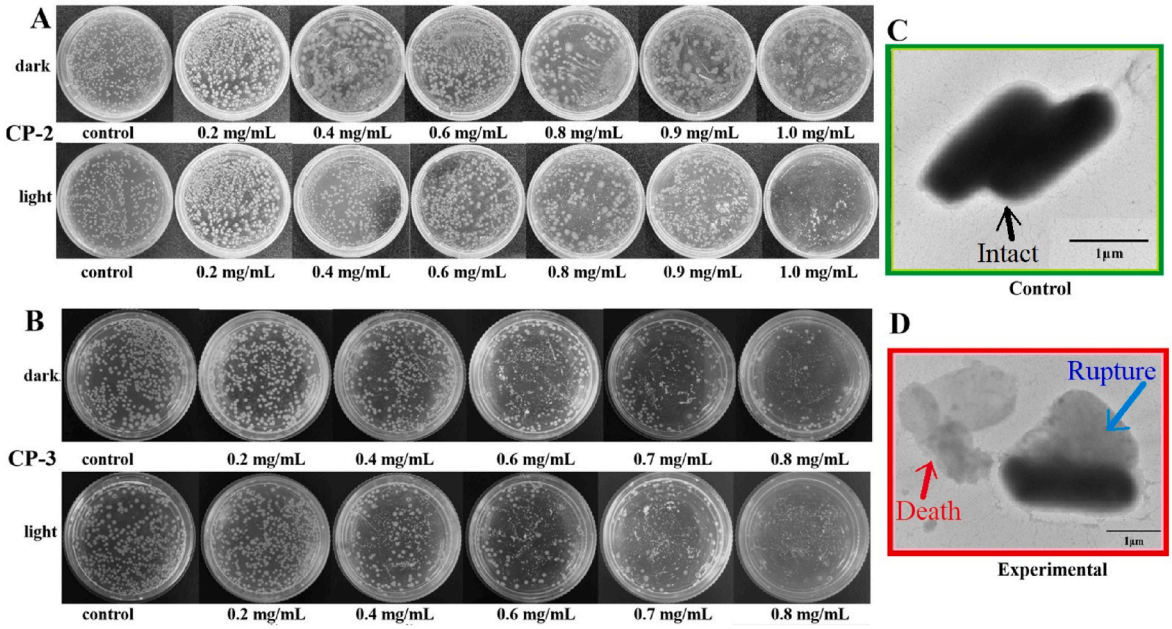

Fig. 4. (A) and (B) photographs illustrating the antibacterial effects of USC-CP-2 and USC-CP-3 at various concentrations against *E. coli* cells, measured using the spread plate method; (C) and (D) TEM images of *E. coli* cells before and after treatment with USC-CP-3.

59.46 to 8.94 CFU/cm^2 in the dark, and from 46.88 to 0 CFU/cm^2 under light exposure. CP-3 exhibited a similar antibacterial trend (Fig. 4B). As the concentration of CP-3 increased from 0 to 0.8 mg/mL, the remaining bacterial colony counts of *E. coli*, as shown in Table S5, decreased from 50.42 to 6.96 CFU/cm^2 in the dark, and from 40.09 to 0.62 CFU/cm^2 under light exposure. Under light conditions, CP-3 demonstrated superior antibacterial activity, achieving a lower MIC value of 0.8 mg/mL, compared to 1.0 mg/mL for CP-2. This indicates that CP-3 is more effective, particularly in the presence of light. These results clearly demonstrate that both coordination polymers exhibit enhanced photodynamic effects, comparable to those of previously reported silver complexes, highlighting their potential as effective antibacterial agents [16,44].

3.4. TEM and SEM observations of bacteria

The morphological changes induced by the coordination polymers USC-CP-2 and USC-CP-3 on *E. coli* cells were systematically analyzed using TEM and SEM. As shown in Fig. 4C, untreated *E. coli* cells maintained intact structures and normal morphology. In contrast, cells treated with USC-CP-3 exhibited severe structural damage and significant morphological alterations (Fig. 4D). TEM images further revealed that *E. coli* cells co-incubated with USC-CP-2 single crystals lost cellular cohesion, with extensive outer membrane damage or complete destruction (Fig. S3 and Fig. S4). Additionally, SEM images (Fig. S5 and Fig. S6) demonstrated that the fine crystalline powders of USC-CP-2 and USC-CP-3 effectively disrupted the bacterial cell wall, ultimately leading to cell death, consistent with the TEM observations.

3.5. Mechanistic study of bactericidal activity

The germicidal effect of Ag(I) complexes is well known to result from physical contact, metal ion/ligand sterilization, oxidative stress, and photothermal effects [1–5,11–16,51]. However, it remains unclear whether the antimicrobial mechanism is driven by any single factor or by the synergistic action of multiple factors. To better understand the internal antibacterial behavior of the two coordination polymers under dark conditions and in the presence of light, electron paramagnetic resonance (EPR) and ICP-MS studies were systematically conducted.

5,5-dimethyl-1-pyrroline N-oxide (DMPO)-trapped EPR experiments were carried out to identify the active species produced by both coordination polymers. As shown in Fig. 5, characteristic signals of hydroxyl radicals (•OH) were detected under LED irradiation (400–700 nm), but not under dark conditions, which demonstrates that the coordination polymers generate •OH radicals upon illumination. Under dark conditions, their antibacterial properties are primarily attributed to the slow release of Ag(I) ions. These results are consistent with previous reports on Ag-MOF antibacterial agents [41,52,53]. In the presence of light, the enhanced antibacterial activity is ascribed to the generation of hydroxyl radicals along with the continuous Ag(I) release, leading to stronger antimicrobial effects.

Based on structural analysis, the weight percentage of Ag(I) in USC-CP-3 is lower than that in USC-CP-2, with values of 53.29 and 54.74 wt %, respectively. Because of the strong Ag-S bond (Ag^+ is a soft acid and *St*Bu is a soft base), the release amount of Ag^+ ions is small. In order to accurately determine their content, ICP-MS was employed. The data showed that the concentrations of Ag(I) ions released were 1.11 mg/L for USC-CP-2 and 5.71 mg/L for USC-CP-3 (Fig. 5C), corresponding to 10.3 and 52.9 mM, respectively, both well below the approximately 600 mM of a 3D Ag-MOF [54]. The higher Ag(I) release from USC-CP-3 is attributed to the relatively weaker Ag-S bonds and the reduced structural stability of the iodide ions trapped in Ag_{16}-cages.

The antibacterial activity of USC-CP-2 operates through two primary mechanisms: the release of intrinsic Ag^+ ions and the generation of •OH radicals, both of which serve as active agents in bacterial eradication. In contrast, USC-CP-3 releases iodide ions encapsulated within Ag_{16}-cages, contributing to a three-in-one synergistic antibacterial mechanism. This combined effect, along with iodide ion release, enhances the bactericidal efficacy of USC-CP-3, making it superior to USC-CP-2. It is well established that antimicrobials with multiple mechanisms of action are more effective in combating drug resistance [55,56]. By targeting bacteria through diverse pathways, they minimize the risk of resistance development, as bacteria are less likely to simultaneously evade multiple mechanisms. Furthermore, synergistic interactions, such as membrane disruption enhancing drug uptake, further amplify efficacy while reducing the likelihood of resistance [56]. By integrating multiple antimicrobial mechanisms, USC-CP-3 addresses a critical gap in current strategies, which often rely on single- or dual-mechanism agents that are

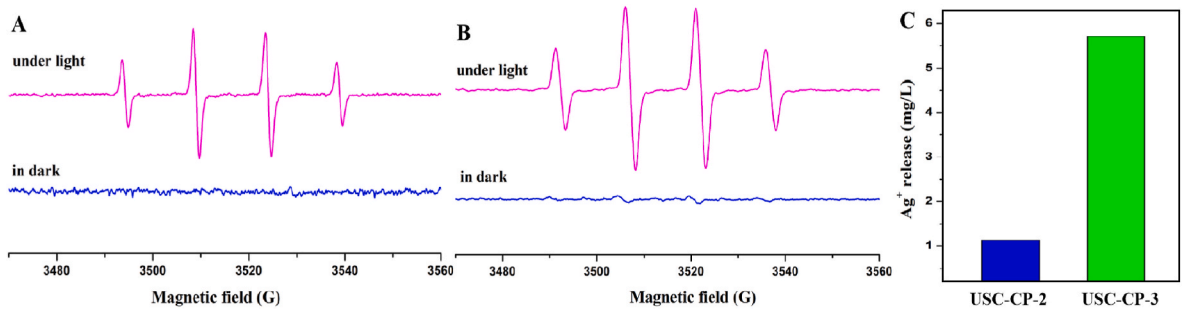

Fig. 5. (A) EPR spectra of DMPO with USC-CP-2; (B) EPR spectra of DMPO with USC-CP-3; and (C) ICP-MS analysis of Ag^+ ion release concentrations.

more susceptible to resistance.

4. Conclusions

In this study, two Ag(I)-thiolate coordination polymers were synthesized using multinuclear Ag(I) nanocages as building blocks, with or without encapsulated iodide ions. $[Ag_6(\mu\text{-}St\text{Bu})_6]_n$ (USC-CP-2) featured a chain-like structure composed of discrete Ag_6-cage units linked by μ_2-*St*Bu ligands, while $[Ag_{14}(\mu\text{-}St\text{Bu})_{12}I_2]_n$ (USC-CP-3) was constructed with edge-shared Ag_{16}-cages containing two encapsulated iodide ions. Both coordination polymers demonstrated significant antibacterial efficacy against Gram-negative bacterium *Escherichia coli*. For USC-CP-2, which lacks iodide ions, the antibacterial activity was primarily ascribed to the gradual release of Ag(I) ions and the generation of hydroxyl radicals under light conditions, leading to moderate antimicrobial activity (MIC value of 1.0 mg/mL). In contrast, USC-CP-3, with iodide ions trapped in its Ag_{16}-cages, exhibited enhanced antimicrobial activity due to a three-in-one antimicrobial mechanism involving Ag(I) release, hydroxyl radical production, and iodide release (MIC value of 0.8 mg/mL). This synergistic interaction between the Ag(I) coordinated 0-D nano-cage and 1-D nano-chain structures provided the materials with both suitable stability and exceptional antimicrobial potency. Overall, this study highlights the potential of these newly developed materials as effective solutions for mitigating bacterial contamination, addressing a critical challenge to public health and disease control. Looking ahead, several key areas require further investigation to advance the practical application of USC-CP-3. Biocompatibility studies are essential to assess its safety for medical use, while environmental impact assessments are needed to evaluate its persistence and degradation in real-world settings. These investigations will not only validate the practical utility of USC-CP-3 but also contribute to the development of next-generation antimicrobial agents capable of combating the growing threat of drug-resistant infections.

CRediT authorship contribution statement

Chunhong Tan: Writing – original draft, Investigation, Conceptualization. **Menghan Lu:** Writing – original draft, Investigation, Formal analysis. **Tao Zhou:** Writing – original draft, Investigation. **Zhen Fang:** Writing – original draft, Investigation, Data curation, Conceptualization. **Juan Zhou:** Writing – original draft, Investigation. **Xiao-Feng Wang:** Writing – review & editing, Writing – original draft, Supervision, Formal analysis, Conceptualization. **Guoqing Wang:** Writing – review & editing, Writing – original draft, Supervision, Funding acquisition, Conceptualization. **Ying-Wu Lin:** Writing – original draft, Validation, Supervision, Funding acquisition. **João Rocha:** Writing – review & editing, Funding acquisition, Conceptualization.

Data availability

Crystallographic data for USC-CP-2 and USC-CP-3 have been deposited at the Cambridge Crystallographic Data Centre (CCDC No. 1853312 and 1853313) and can be obtained free of charge via www.ccdc.cam.ac.uk/data_request/cif, data_request@ccdc.cam.ac.uk or by contacting The Cambridge Crystallographic Data Centre, 12 Union Road, Cambridge CB2 1EZ, UK; fax: +44 1223 336033, format https://doi.org/DOI].

Declaration of competing interest

The authors declare that they have no known competing financial interests or personal relationships that could have appeared to influence the work reported in this paper.

Acknowledgements

This work was financially supported by the National Natural Science Foundation of China (12405385 and 32373172), the Provincial Natural Science Foundation of Hunan (2021JJ30565), and the China Scholarship Council (202202505005). JR thanks the project CICECO-Aveiro Institute of Materials, Grants UIDB/50011/2020, UIDP/50011/2020 and LA/P/0006/2020, financed by national funds through the FCT/MEC (PIDDAC).

Appendix A. Supplementary data

Supplementary data to this article can be found online at https://doi.org/10.1016/j.mtbio.2025.101673.

Data availability

Data will be made available on request.

References

[1] O. Pacios, L. Blasco, I. Bleriot, L. Fernandez-Garcia, M.G. Bardanca, A. Ambroa, M. López, G. Bou, M. Tomas, Strategies to combat multidrug-resistant and persistent infectious diseases, Antibiot. 9 (2020) 20–38.
[2] A.J. Muñoz, F. Espinola, E. Ruiz, M. Moya, E. Castro, Biocidal and synergistic effect of three types of biologically synthesised silver/silver chloride nanoparticles, World J. Microbiol. Biotechnol. 40 (2024) 14–20.
[3] S. Agnihotri, S. Mukherji, S. Mukherji, Impact of background water quality on disinfection performance and silver release of immobilized silver nanoparticles: modeling disinfection kinetics, bactericidal mechanism and aggregation behavior, Chem. Eng. J. 372 (2019) 684–696.
[4] M.K. Annavajhala, A. Gomez-Simmonds, N. Macesic, S.B. Sullivan, A. Kress, S. D. Khan, M.J. Giddins, S. Stump, G.I. Kim, R. Narain, E.C. Verna, A.C. Uhlemann, Colonizing multidrug-resistant bacteria and the longitudinal evolution of the intestinal microbiome after liver transplantation, Nat. Commun. 10 (2019) 4715.
[5] J.L.M. Christopher, et al., Global burden of bacterial antimicrobial resistance in 2019: a systematic analysis, Lancet 399 (2022) 629–655.
[6] H. Shabani, M.H. Karami, J. Kolour, Z. Sayyahi, M.A. Parvin, S. Soghala, S. S. Baghini, M. Mardasi, A. Chopani, P. Moulavi, T. Farkhondeh, M. Darroudi, M. Kabiri, S. Samarghandian, Anticancer activity of thymoquinone against breast cancer cells: mechanisms of action and delivery approaches, Biomed. Pharmacother. 165 (2023) 114972–114979.
[7] Z. Sabouri, S. Sammak, S. Sabouri, S.S. Tabrizi Hafez Moghaddas, M. Darroudi, Green synthesis of Ag-Se doped ZnO-Co_3O_4-NiO quinary nanocomposite using poly anionic cellulose and evaluation of their anticancer and photocatalyst applications, Chem. Methodol. 8 (2024) 164–176.

[8] R. Hazrati Saadabadia, F. Shariatmadar Tehrani, M. Darroudi, Z. Sabouri, Plant-based synthesis of ZnO-CeO_2-MgO nanocomposite using *Ocimum Basilicum* L seed extract: biological effects and photocatalytic activity, Mater. Chem. Phys. 314 (2024) 128919.

[9] Z. Sabouri, M. Sabouri, S.S.T.H. Moghaddas, A. Mostafapour, S. Samarghandian, M. Darroudi, Plant-mediated synthesis of Ag and Se dual-doped ZnO-CaO-CuO nanocomposite using *Nymphaea alba L.* extract: assessment of their photocatalytic and biological properties, Biomass Convers. Bior. 14 (2024) 32121–32131.

[10] M. Mohtashami, A. Rezagholizade-Shirvan, Z.H. Bonab, M. Amiryousefi, M. Darroudi, M.A. Solimani, Green synthesis of silver nanoparticles using cirsium congestum extract modified by chitosan/alginate: bactericidal activity against pathogenic bacteria and cytotoxicity analysis in normal cell line, Curr. Pharm. Des. 20 (2024) 30–43.

[11] J.X. Guan, J.L. Wang, F.Z. Jia, W.J. Jiang, L.L. Song, L. Xie, H. Yang, P.D. Han, H. Lin, Z.Z. Wu, X.J. Zhang, Y. Huang, Layer-by-layer self-assembly coatings on strontium titanate nanotubes with antimicrobial and anti-inflammatory properties to prevent implant-related infections, Colloids Surf., B 244 (2024) 114183–114192.

[12] D.Y. Xu, X.F. Wang, M.Y. Li, L. Xie, K.J. Liu, Y.H. Liu, J.P. Lan, P.D. Han, H. Lin, L. L. Song, X.J. Zhang, Y. Huang, Enhancing titanium-osteointegration: antimicrobial, anti-inflammatory and osteogenic properties of multifunctional coatings through layer-by-layer self-assembly, Appl. Surf. Sci. 686 (2025) 162149–162158.

[13] F.Z. Jia, J.X. Guan, J.L. Wang, M.Y. Li, Y.S. Zhang, L. Xie, P.D. Han, H. Lin, X. Huang, J.P. Lan, Y. Huang, Zinc and melatonin mediated antimicrobial, anti-inflammatory, and antioxidant coatings accelerate bone defect repair, Colloids Surf., B 245 (2025) 114335–114343.

[14] J.L. Wang, J.X. Guan, F.Z. Jia, Z.T. Tian, L.L. Song, L. Xie, P.D. Han, H. Lin, H. X. Qiao, X.J. Zhang, Y. Huang, Phase-transformed lactoferrin/strontium-doped nanocoatings enhance antibacterial, anti-inflammatory and vascularised osteogenesis of titanium, Int. J. Biol. Macromol. 287 (2025) 138608–138614.

[15] B.B. Wang, J.P. Lan, H.X. Qiao, L. Xie, H. Yang, H. Lin, Xiaoming Li, Yong Huang, Porous surface with fusion peptides embedded in strontium titanate nanotubes elevates osteogenic and antibacterial activity of additively manufactured titanium alloy, Colloids Surf., B 224 (2023) 113188–113196.

[16] J.H. Liu, D. Wu, N. Zhu, Y.N. Wu, G.L. Li, Antibacterial mechanisms and applications of metal-organic frameworks and their derived nanomaterials, Trends Food Sci. Technol. 109 (2021) 413–434.

[17] M. Hajibabaei, R. Zendehdel, Z. Panjali, Imidazole-functionalized Ag/MOFs as promising scaffolds for proper antibacterial activity and toxicity reduction of Ag nanoparticles, J. Inorg. Organomet. Polym. Mater. 30 (2020) 4622–4626.

[18] A. Pöthig, S. Ahmed, H.C. Winther-Larsen, S.Y. Guan, P.J. Altmann, J. Kudermann, A.M.S. Andresen, T. Gjoen, O.A.H. Åstrand, Antimicrobial activity and cytotoxicity of Ag(I) and Au(I) pillarplexes, Front. Chem. 6 (2018) 8–17.

[19] W. Qian, H.K. Yuan, R. Zhang, R.Q. Fang, Silver(I) complexes with halo-substituted cyanoanilines: synthesis, characterization and antibacterial activity, J. Coord. Chem. 69 (2016) 3593–3602.

[20] Y.M. Wu, P.C. Zhao, B. Jia, Z. Li, S. Yuan, C.H. Li, A silver-functionalized metal-organic framework with effective antibacterial activity, New J. Chem. 46 (2022) 5922–5926.

[21] J.H. Jo, H.C. Kim, S. Huh, Y. Kim, D.N. Lee, Antibacterial activities of Cu-MOFs containing glutarates and bipyridyl ligands, Dalton Trans. 48 (2019) 8084–8093.

[22] Y.H. Guo, C.M. Dundas, X.Y. Zhou, K.P. Johnston, G.H. Yu, Molecular engineering of hydrogels for rapid water disinfection and sustainable solar vapor generation, Adv. Mater. 33 (2021) 8–15.

[23] J. Song, C.Q. Zhang, S.W. Kong, F.Y. Liu, W.J. Hu, F. Su, S.M. Li, Novel chitosan-based metal-organic polyhedrons/enzyme hybrid hydrogel with antibacterial activity to promote wound healing, Carbohydr. Polym. 291 (2022) 119522–119530.

[24] D.L. Han, X.M. Liu, S.L. Wu, Metal organic framework-based antibacterial agents and their underlying mechanisms, Chem. Soc. Rev. 51 (2022) 7138–7169.

[25] Z.X. Pan, Y.Y. Fu, C. Peng, L. Xiao, S.R. Zhu, F.J. Peng, Q. Liu, B.L. Zhou, Triazine-Porphyrin-based aminal linked porous organic polymer as self-enhanced photo/enzyme synergistic antibacterial agent for wound healing, Microporous Mesoporous Mater. 365 (2024) 112881–112889.

[26] A.S.K. Kumar, W.B. Tseng, E. Arputharaj, P.J. Huang, W.L. Tseng, T. Bajda, Covalent organic framework nanosheets as an enhancer for light-responsive oxidase-like nanozymes: multifunctional applications in colorimetric sensing, antibiotic degradation, and antibacterial agents, ACS Sustain. Chem. Eng. 11 (18) (2023) 6956–6969.

[27] F.L. Ran, C.Y. Li, Z.X. Hao, X.Y. Zhang, L. Dai, C.L. Si, Z.Q. Shen, Z.G. Qiu, J. F. Wang, Combined bactericidal process of lignin and silver in a hybrid nanoparticle on *E. coli*, Adv. Compos. Hybrid Mater. 5 (2022) 1841–1851.

[28] P.N. Catalano, M. Pezzoni, C. Costa, G. Soler-Illia, M.G. Bellino, M.F. Desimone, Optically transparent silver-loaded mesoporous thin film coating with long-lasting antibacterial activity, Microporous Mesoporous Mater. 236 (2016) 158–166.

[29] W. Sim, R.T. Barnard, M.A.T. Blaskovich, Z.M. Ziora, Antimicrobial silver in medicinal and consumer applications: a patent review of the past decade (2007-2017), Antibiot. 7 (2018) 93–107.

[30] J.W. Alexander, History of the medical use of silver, Surg. Infect. 10 (2009) 289–292.

[31] S. Anees Ahmad, S. Sachi Das, A. Khatoon, M. Tahir Ansari, M. Afzal, M. Saquib Hasnain, A. Kumar Nayak, Bactericidal activity of silver nanoparticles: a mechanistic review, Mater. Sci. Energy Technol. 3 (2020) 756–769.

[32] M. Carvalho, S. Leite, J.P. Costa, A.M. Galvao, J.H. Leitao, Ag(I) camphor complexes: antimicrobial activity by design, J. Inorg. Biochem. 199 (2019) 110791–110799.

[33] A.J. Muñoz, F. Espínola, E. Ruiz, M. Moya, E. Castro, Biocidal and synergistic effect of three types of biologically synthesised silver/silver chloride nanoparticles, World J. Microbiol. Biotechnol. 40 (2024) 1–18.

[34] C.Z. Liao, Y.C. Li, S.C. Tjong, Bactericidal and cytotoxic properties of silver nanoparticles, Int. J. Mol. Sci. 20 (2019) 449–495.

[35] K. Verduzco-Chavira, A.A. Vallejo-Cardona, A.S. González-Garibay, O.R. Torres-González, I.M. Sánchez-Hernández, J.M. Flores-Fernández, E. Padilla-Camberos, Antibacterial and antibiofilm activity of chemically and biologically synthesized silver nanoparticles, Antibiot. 12 (2023) 1084–1090.

[36] W.F. Zhang, G.M. Ye, D.H. Liao, X.L. Chen, C.Y. Lu, A. Nezamzadeh-Ejhieh, M. S. Khan, J.Q. Liu, Y. Pan, Z. Dai, Recent advances of silver-based coordination polymers on antibacterial applications, Molecules 27 (2022) 27–33.

[37] J.H.B. Nunes, D.H. Nakahata, P.P. Corbi, R. Paiva, Beyond silver sulfadiazine: a dive into more than 50 years of research and development on metal complexes of sulfonamides in medicinal inorganic chemistry, Coord. Chem. Rev. 490 (2023) 1–45.

[38] S. Medici, M. Peana, G. Crisponi, V.M. Nurchi, J.I. Lachowicz, M. Remelli, M. A. Zoroddu, Silver coordination compounds: a new horizon in medicine, Coord. Chem. Rev. 327 (2016) 349–359.

[39] M. Bosetti, A. Masse, E. Tobin, M. Cannas, Silver coated materials for external fixation devices: in vitro biocompatibility and genotoxicity, Biomaterials 23 (2002) 887–892.

[40] P. Wu, D.W. Grainger, Drug/device combinations for local drug therapies and infection prophylaxis, Biomaterials 27 (2006) 2450–2467.

[41] R. Jin, C. Zeng, M. Zhou, Y. Chen, Atomically precise colloidal metal nanoclusters and nanoparticles: fundamentals and opportunities, Chem. Rev. (2016) 10346–10413.

[42] J.F. Corrigan, O. Fuhr, D. Fenske, Metal chalcogenide clusters on the border between molecules and materials, Adv. Mater. 21 (2009) 1867–1871.

[43] O. Fuhr, S. Dehnen, D. Fenske, Chalcogenide clusters of copper and silver from silylated chalcogenide sources, Chem. Soc. Rev. 42 (2013) 1871–1906.

[44] B. Krebs, G. Henkel, Transition metal thiolates: from molecular fragments of sulfidic solids to models for active centers in biomolecules, Angew. Chem. Int. Ed. 30 (1991) 769–788.

[45] X.Y. Lu, J.W. Ye, Y. Sun, R.F. Bogale, L.M. Zhao, P. Tian, G.L. Ning, Ligand effects on the structural dimensionality and antibacterial activities of silver-based coordination polymers, Dalton Trans. 43 (2014) 10104–10113.

[46] A.N. Au-Duong, C.K. Lee, Iodine-loaded metal organic framework as growth-triggered antimicrobial agent, Mater. Sci. Eng. C 76 (2017) 477–482.

[47] X. Han, G. Boix, M. Balcerzak, O.H. Moriones, M. Cano-Sarabia, P. Cortés, N. Bastús, V. Puntes, M. Llagostera, I. Imaz, D. Maspoch, Antibacterial films based on MOF composites that release iodine passively or upon triggering by near-infrared light, Adv. Funct. Mater. 32 (2022) 2112902–2112913.

[48] G. McDonnell, A.D. Russell, Antiseptics and disinfectants: activity, action, and resistance, Clin. Microbiol. Rev. 12 (1999) 147–179.

[49] Q. Wang, S.L. Dong, D.D. Tao, Z. Li, Y.B. Jiang, Ag(I)-thiolate coordination polymers: synthesis, structures and applications as emerging sensory ensembles, Coord. Chem. Rev. 432 (2021) 213717–213734.

[50] N. Kaur, P. Tiwari, K.S. Kapoor, A.K. Saini, V. Sharma, S.M. Mobin, Metal-organic framework based antibiotic release and antimicrobial response: an overview, CrystEngComm 22 (2020) 7513–7527.

[51] M. Yang, J. Zhang, Y.H. Wei, J. Zhang, C.M. Tao, Recent advances in metal-organic framework-based materials for anti-staphylococcus aureus infection, Nano Res. 15 (2022) 6220–6242.

[52] Y.P. Xie, J.L. Jin, X. Lu, T.C.W. Mak, High-nuclearity silver thiolate clusters constructed with phosphonates, Angew. Chem. Int. Ed. 54 (2015) 15176–15180.

[53] C. Healy, W. Schmitt, Multicomponent halide templating: the effect of structure-directing agents on the assembly of molecular and extended coordination compounds, Coord. Chem. Rev. 371 (2018) 67–85.

[54] M. Berchel, T. Le Gall, C. Denis, S. Le Hir, F. Quentel, C. Elleouet, T. Montier, J. M. Rueff, J.Y. Salaun, J.P. Haelters, G.B. Hix, P. Lehn, P.A. Jaffres, A silver-based metal-organic framework material as a 'reservoir' of bactericidal metal ions, New J. Chem. 35 (2011) 1000–1003.

[55] Y.Y. He, X. Wang, S.S. He, X.L. Han, A. Wang, F.J. Zhang, J.L. Deng, X.R. Long, J. J. Lin, Y. Feng, X.L. He, Z. Li, J.H. Li, F. Luo, H. Tan, Enhancing antibiotic-resistant bacterial infection therapy: self-assembling gemini quaternary ammonium-functionalized peptide nanoassemblies with multiple antibacterial mechanisms, ACS Nano 19 (2025) 6977–6992.

[56] G. Jain, R. Chaurasia, B.P. Kaur, O.P. Chowdhury, H. Roy, R.R. Gupta, B. Biswas, S. Chakrabarti, M. Mukherjee, Unleashing the antibacterial Potential of ZIFs and their derivatives: mechanistic insights, J. Mater. Chem. B 13 (2025) 3270–3291.